

# Exploring differential two-particle correlations in $\gamma p$ and low-multiplicity pp collisions using PYTHIA8

Subash Chandra Behera<sup>1,\*</sup> and Dukhishyam Mallick<sup>2,†</sup>

<sup>1</sup>*INFN-Sezione di Roma, Piazzale Aldo Moro, 2-00185 Rome, Italy*

<sup>2</sup>*INFN-Sezione di Cagliari, Monserrato, 09042, Cagliari, Italy*

A study of two-particle differential number ( $B$ ) and transverse momentum ( $P_2^{\text{CD}}$ ) balance functions in photon-proton ( $\gamma p$ ) and proton-proton (pp) collisions at  $\sqrt{s} = 5.36$  TeV is presented. The analysis focuses on inclusive charged hadrons within the pseudorapidity coverage  $|\eta| < 2.4$  and the transverse momentum interval  $0.3 < p_T < 3.0$  GeV and examines their correlations in terms of relative pseudorapidity ( $\Delta\eta$ ) and relative azimuthal angle ( $\Delta\phi$ ). The correlation functions are evaluated for same- and opposite-sign pairs, and their combinations are used to extract charge-dependent (CD) and charge-independent (CI) components. The evolution of the near-side peak of the CD correlations is investigated in terms of  $\Delta\eta$  and  $\Delta\phi$  as a function of charged-particle multiplicity ( $N_{\text{ch}}$ ) for  $\gamma p$  collisions and compared to pp collisions at a similar multiplicity range. A clear multiplicity dependence of the balance-function width is obtained. The width is found systematically lower in  $\gamma p$  events than in pp collisions. This study provides valuable information on particle correlations and production mechanisms in low- $N_{\text{ch}}$  regimes for upcoming measurements in small systems.

## I. INTRODUCTION

Measurements from ultra-relativistic heavy-ion collisions at the Relativistic Heavy Ion Collider (RHIC) and the Large Hadron Collider (LHC) have provided compelling evidence for the formation of a strongly interacting matter known as the quark-gluon plasma (QGP) [1–7]. The observation of pronounced collective flow, especially the large elliptic flow coefficient ( $v_2$ ), has been observed. Theoretical descriptions based on relativistic hydrodynamics suggest that the QGP behaves like an almost perfect fluid with extremely low shear viscosity [8]. Studying correlations between oppositely charged particle pairs created in heavy-ion collisions provides insight into the dynamics of the QGP and the underlying hadronization mechanism [9–17]. The particle production is governed by local charge conservation, in which the creation of a positively charged particle must be accompanied by the production of a negatively charged partner. The balance function is designed to quantify the correlations in phase space variables such as pseudorapidity difference ( $\Delta\eta$ ) and azimuthal angle difference ( $\Delta\phi$ ) [10–13, 15, 18–22].

Measurements of the near-side peak width of the charge balance function exhibit a strong system-size dependence across various collision systems spanning over RHIC to LHC energies [16–19].

A significant narrowing of the balance functions width are observed in central heavy-ion collisions. This effect is interpreted as the signature of delayed hadronization in the presence of the QGP medium, where balancing charges are produced at a later stage of the system evolution and therefore remain closer in phase space [16–19].

Recent observations of long-range rapidity correlations (“ridge-like” structures), non-zero flow harmonics, and the narrowing of the near-side width of the correlation functions in small collision systems exhibit features qualitatively similar to those seen in heavy-ion collisions [3, 23–27]. The unexpected narrowing behavior challenges the conventional interpretation associated with delayed hadronization in the deconfined medium. As a result, the mechanism responsible for this behavior in small systems remains not fully understood [24, 27, 28].

Several theoretical studies using event generators such as PYTHIA8, AMPT, and EPOS, which incorporate distinct physics mechanisms including string fragmentation, partonic transport, and hydrodynamic evolution also reproduce the similar decreasing trend of the balance-function width with increasing multiplicity [13, 18, 29–31]. This suggests that multiple mechanisms, such as local charge conservation, string dynamics, multiple parton interactions (MPI), color reconnection, or parton transport effects, may contribute to the observed behavior.

In this work, the correlation functions are

\* Contact author: subash.chandra.behera@cern.ch

† Contact author: dukhishyam.mallick@cern.ch

further investigated in even smaller collision systems, extending to photon-induced  $\gamma p$  collisions using PYTHIA8 simulations [32, 33]. Such collisions provide a cleaner environment compared to hadronic pp interactions, as electromagnetic processes dominate and the underlying hadronic event activity is significantly [34, 35]. These events are characterized by very low charged-particle multiplicity due to the suppression of the MPI and the absence of an extended QGP-like medium. Therefore,  $\gamma p$  collisions offer an ideal baseline for studying correlation functions and disentangling genuine charge conservation effects from medium-induced phenomena observed in hadronic collisions.

In this work, both charge-independent (CI) and charge-dependent (CD) two-particle number and transverse-momentum ( $p_T$ ) correlations are presented. The focus of this study is the CD correlation, which isolates correlations associated with charge conservation by subtracting like-sign pair contributions from unlike-sign pairs. Then, to quantify the correlation strength, the root-mean-square widths of the CD correlation functions are extracted from their one-dimensional distributions onto  $\Delta\eta$  and  $\Delta\phi$ .

This paper is organized as follows. Section II describes the analysis methodology. Section III discusses the model setup and framework used for this study. Section IV presents the results for  $B$ ,  $P_2^{\text{CD}}$  correlations, and their corresponding widths in  $\Delta\eta$  and  $\Delta\phi$ . Finally, Section V summarizes this work. The additional discussions about the CI correlations can be found in Section VI.

## II. ANALYSIS METHODOLOGY

Two-particle number correlation functions,  $C_2$  are constructed using the “trigger” and “associated” tracks that are selected from the same event. Both the trigger and associated particles are selected in  $|\eta| < 2.4$  and  $0.3 < p_T < 3.0$  GeV intervals. For each pair, the differences in  $\Delta\eta$  and  $\Delta\phi$  are calculated. The per-trigger associated yield in the same event is defined as

$$S(\Delta\eta, \Delta\phi) = \frac{1}{N_{\text{trig}}} \frac{d^2 N^{\text{same}}}{d\Delta\eta d\Delta\phi}, \quad (1)$$

where  $N_{\text{trig}}$  is the number of trigger particles and  $N^{\text{same}}$  is the number of same-event pairs. The

mixed-event distributions are calculated by randomly mixing six chosen events in the similar multiplicity class for  $0.3 < p_T < 3.0$  GeV and  $|\eta| < 2.4$  intervals. This can be written as

$$M(\Delta\eta, \Delta\phi) = \frac{1}{N_{\text{trig}}} \frac{d^2 N^{\text{mix}}}{d\Delta\eta d\Delta\phi}, \quad (2)$$

where  $N^{\text{mix}}$  denotes the number of mixed-event pairs. The mixed-event background distribution accounts for the finite detector acceptance and pair efficiency [18, 19, 23, 25, 26, 29, 34]. The two-particle number correlation function is then obtained as the ratio of the same-event signal to the mixed-event background [18, 19, 23, 25, 26, 29, 34].

$$\frac{1}{N_{\text{trig}}} \frac{d^2 N^{\text{pair}}}{d\Delta\eta d\Delta\phi} = C_2(\Delta\eta, \Delta\phi) \quad (3)$$

$$= M(0, 0) \frac{S(\Delta\eta, \Delta\phi)}{M(\Delta\eta, \Delta\phi)}. \quad (4)$$

The term  $M(0, 0)/M(\Delta\eta, \Delta\phi)$  mainly accounts for the pair acceptance effects and  $M(0, 0)$  denotes the mixed-event yield when both particles are emitted approximately in the same direction, leading to the highest pair detection efficiency.

Similarly, the two-particle transverse momentum correlator,  $P_2$  that takes care of  $p_T$  fluctuations can be defined as

$$P_2(\Delta\eta, \Delta\phi) = \frac{\langle \Delta p_T \Delta p_T \rangle(\Delta\eta, \Delta\phi)}{\langle p_T \rangle^2}, \quad (5)$$

where  $\Delta p_T = p_T - \langle p_T \rangle$  and  $\langle \Delta p_T \Delta p_T \rangle$  is the differential correlator can be defined as

$$\langle \Delta p_T \Delta p_T \rangle(\Delta\eta, \Delta\phi) = \frac{\int_{p_{T,\text{min}}}^{p_{T,\text{max}}} \Delta p_T \Delta p_T c'_2(\vec{p}_1, \vec{p}_2) dp_T dp_T}{\int_{p_{T,\text{min}}}^{p_{T,\text{max}}} c'_2(\vec{p}_1, \vec{p}_2) dp_T dp_T}, \quad (6)$$

where  $c'_2$  is the two-particle density distribution, expressed as a function of the transverse momenta. The momentum correlator is normalized  $\langle p_T \rangle^2$  to make the  $P_2$  correlation dimensionless. The  $P_2$  correlation is influenced by the presence of number correlations and the transverse momentum distribution of the correlated particle pairs, and the details can be found in Ref. [14, 15, 29].

The CI and CD components are constructed using  $C_2$  and  $P_2$  correlation functions from their corresponding same-sign (SS) and opposite-sign (OS) pairs. The CI correlation is the average of SS and OS correlation functions, and the CD correlation

is the difference of the SS and OS correlation functions. The SS and OS pairs are influenced by different physical mechanisms, taking their combination can isolate the correlation associated with balancing charges. This effect is quantified through the CD correlation. Mathematically, these components are expressed as follows:

$$C_2^{\text{CI}} = \frac{1}{2}[C_2^{(+,-)} + C_2^{(-,+)} + C_2^{(-,-)} + C_2^{(+,+)}]. \quad (7)$$

$$P_2^{\text{CI}} = \frac{1}{2}[P_2^{(+,-)} + P_2^{(-,+)} + P_2^{(-,-)} + P_2^{(+,+)}]. \quad (8)$$

$$B = \frac{1}{2}[C_2^{(+,-)} + C_2^{(-,+)} - C_2^{(-,-)} - C_2^{(+,+)}]. \quad (9)$$

$$P_2^{\text{CD}} = \frac{1}{2}[P_2^{(+,-)} + P_2^{(-,+)} - P_2^{(-,-)} - P_2^{(+,+)}]. \quad (10)$$

The strength of the balance functions is quantified by the root-mean-square (RMS) width of their one-dimensional (1D) projections onto  $\Delta\eta$  and  $\Delta\phi$ . The 1D  $\Delta\eta$  and  $\Delta\phi$  distributions are obtained from the two-dimensional correlation functions by integrating over the intervals  $|\Delta\phi| < \pi/2$  and  $|\Delta\eta| < 1.0$ , respectively. Mathematically, the RMS width ( $\sigma_{\mathcal{O}}$ ) is defined as follows:

$$\sigma_{\mathcal{O}} = \sqrt{\frac{\sum_i \mathcal{O}_i^2 B(\mathcal{O}_i)}{\sum_i B(\mathcal{O}_i)}}, \quad (11)$$

where  $B(\mathcal{O}_i)$  denotes the balance function evaluated in the  $i^{\text{th}}$  bin centered at  $\mathcal{O}_i$ , and  $\mathcal{O}$  represents the relative separation variable, such as  $\Delta\eta$  or  $\Delta\phi$ . The summation runs over all bins within the selected kinematic range. A similar approach is followed to extract the RMS width of  $P_2^{\text{CD}}$  correlations. The  $\sigma_{\Delta\eta}$  and  $\sigma_{\Delta\phi}$  are calculated in  $|\Delta\eta| < 2.0$  and  $|\Delta\phi| < \pi/2$  interval, respectively.

### III. MODEL DESCRIPTION

In this study, events are generated using PYTHIA 8.36 [32, 36] to simulate both  $\gamma p$  and pp collisions, with approximately 0.2 billion and 3 billion events, respectively. For  $\gamma p$  collisions, the photon flux is modeled using the Equivalent Photon Approximation (EPA) implemented in PYTHIA, where the photon is treated as another beam parti-

cle(Beams:idA = 22). The details of the modeling can be found in Ref. [37].

To provide a realistic description of photon-induced interactions and to suppress contributions from underlying-event activity and MPI, all hard QCD processes are disabled (HardQCD:all = off, PartonLevel:MPI = off), while photon-induced processes are enabled (PhotonParton:all = on). In addition, the Monash tune for minimum-bias inelastic pp collisions at LHC energies is considered for comparison. The same tune is also applied to the  $\gamma p$  simulations to study the differences in final-state particle production and production mechanisms when changing the collision system from pp to  $\gamma p$ .

This configuration uses Tune:pp = 14, SoftQCD:inelastic = on, PartonLevel:MPI = on, and ColourReconnection:reconnect = on. This setup is referred to as the MB-like tune throughout this paper.

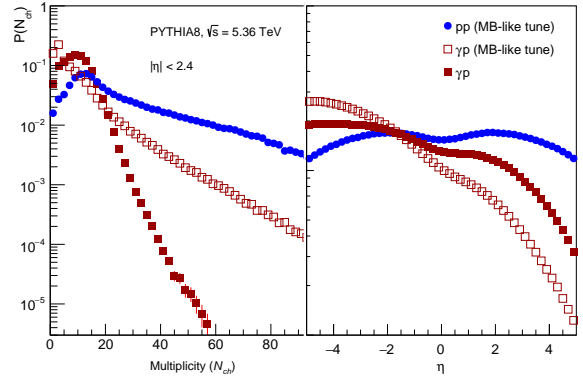


FIG. 1. Comparison of multiplicity ( $N_{\text{ch}}$ ) and pseudorapidity ( $\eta$ ) distributions of charged hadrons in MB pp, MB-like tune  $\gamma p$  and  $\gamma p$  collisions at  $\sqrt{s} = 5.36$  TeV.

Figure 1 illustrates the normalized charged-particle multiplicity ( $N_{\text{ch}}$ , left panel) and pseudorapidity ( $\eta$ , right panel) distributions in pp and  $\gamma p$  collisions from PYTHIA8 simulations. The charged-particle multiplicity distributions for inelastic MB pp collisions show significantly higher values of  $N_{\text{ch}}$  compared to  $\gamma p$  collisions. The distributions are evaluated within the pseudorapidity interval  $|\eta| < 2.4$ . The ordering of the multiplicity spectra is observed as

$$N_{\text{ch}}^{\gamma p} < N_{\text{ch}}^{\gamma p, \text{MB-like}} < N_{\text{ch}}^{pp, \text{MB-like}}. \quad (12)$$

The MB pp collisions reach larger  $N_{\text{ch}}$  values

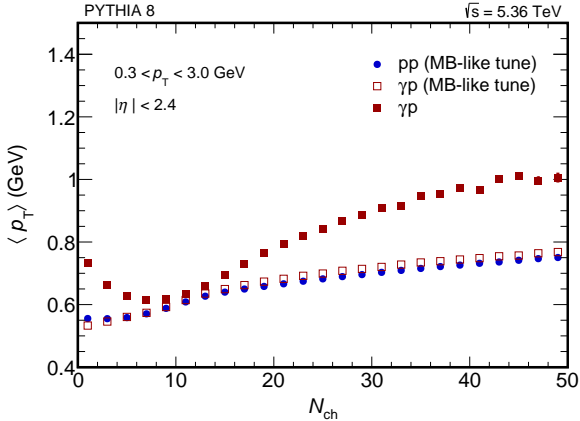


FIG. 2. Comparison of average transverse momentum ( $\langle p_T \rangle$ ) as function of  $N_{ch}$  for charged hadrons in MB pp, MB-like tune  $\gamma p$  and  $\gamma p$  collision at  $\sqrt{s} = 5.36$  TeV. Results are calculated for  $|\eta| < 2.4$  and  $0.3 < p_T < 3.0$  GeV.

and exhibit broader multiplicity distribution due to the presence of multiple partonic interactions, underlying event activities, and the larger available phase space in a fully hadronic system. In contrast, the  $\gamma p$  collisions show lower multiplicity coverage and a rapidly falling distribution with increasing  $N_{ch}$ . This behaviour reflects the more elementary nature of photon-induced interactions, where particle production is typically driven by a single hard or semi-hard scattering process. Although the overall  $N_{ch}$  depends on the collision system, it is also sensitive to the choice of tune and underlying physics processes included in the simulation.

The  $\eta$  distributions are symmetric around midrapidity ( $\eta \sim 0$ ) in pp collisions, whereas an asymmetric shape is observed in  $\gamma p$  collisions. It is expected due to the asymmetric  $\gamma p$  system. The multiplicity coverage is chosen based on the maximum  $N_{ch}$  reach in  $\gamma p$  collisions, and also the similar overlap multiplicity range is considered for pp collisions.

Figure 2 presents the average transverse momentum ( $\langle p_T \rangle$ ), as a function of the  $N_{ch}$  for  $\gamma p$  and pp collisions at  $\sqrt{s} = 5.36$  TeV from PYTHIA8 simulations. The  $\langle p_T \rangle$  are calculated for charged hadrons in the interval  $0.3 < p_T < 3.0$  GeV and within  $|\eta| < 2.4$ . A monotonically increasing behavior of  $\langle p_T \rangle$  with  $N_{ch}$  is observed. The  $\langle p_T \rangle$  values and their dependence on  $N_{ch}$  are found to be similar

between  $\gamma p$  and pp collisions when they have MB-like configurations. However, a steeper rise of  $\langle p_T \rangle$  with  $N_{ch}$  is observed for  $\gamma p$  collisions with a more realistic configuration for photon-induced interaction. The  $\langle p_T \rangle$  values are higher compared to pp collisions at a given multiplicity, and the difference becomes more pronounced at higher  $N_{ch}$ . This indicates that the  $\langle p_T \rangle$  is sensitive to the underlying physics processes and model tunes than to the nature of the colliding systems when comparing pp and  $\gamma p$  collisions. These results demonstrate that the correlation between multiplicity and transverse momentum depends on several components, such as roles of quark- and gluon-initiated interactions, color reconnection, and MPI dynamics.

## IV. RESULTS AND DISCUSSION

### A. Charge-dependent correlations

Figure 3 presents the two-dimensional balance function  $B$  for charged hadrons in terms of  $\Delta\eta$  and  $\Delta\phi$  for two different multiplicity intervals in  $\gamma p$  and pp collisions at  $\sqrt{s} = 5.36$  TeV. The low and high multiplicity correspond to  $0 < N_{ch} < 5$  (upper panels) and  $40 < N_{ch} < 50$  (lower panels), respectively.

At very low multiplicity ( $0 < N_{ch} < 5$ ) in pp and MB-like tune  $\gamma p$  collisions, the balance function exhibits a strong away-side correlation around  $\Delta\phi \approx \pi$ , reflecting the dominance of a single hard parton scattering and the resulting back-to-back dijet topology. As the multiplicity increases, this away-side structure decreases in magnitude due to the growing importance of MPI, while the near-side peak at  $\Delta\eta \approx 0$  becomes significantly stronger, rising from about 0.01 at  $N_{ch} \approx 5$  to approximately 0.1 for  $40 < N_{ch} < 50$ . This behavior is consistent with a transition from long-range charge balancing across dijets at low multiplicity to predominantly local charge conservation (LCC).

However, the results from the  $\gamma p$  collisions (top, right) without MB-like tune of Fig. 3 exhibit different behavior compared to the pp collisions at similar  $N_{ch}$ . At very low multiplicity, the  $B$  shows a much weaker away-side peak, which rapidly disappears with increasing multiplicity. This suppression is attributed to the lack of MPI and hard QCD dijet contributions because the photon interacts predominantly through a single, highly asymmetric color string attached to a quark in

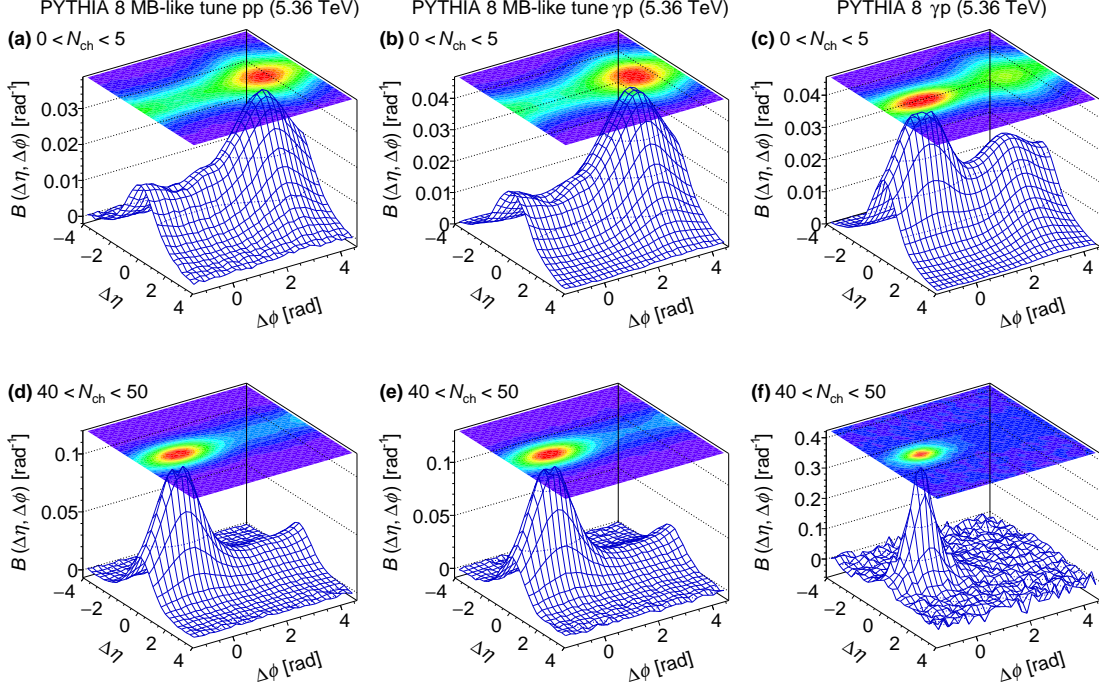


FIG. 3. Two-dimensional number balance functions ( $B$ ) for  $0 < N_{\text{ch}} < 5$  (upper panel) and  $40 < N_{\text{ch}} < 50$  (lower panel) of charged-hadrons in MB-like tune pp (left), MB-like tune  $\gamma p$  (middle), and  $\gamma p$  (right) collisions at  $\sqrt{s} = 5.36$  TeV from PYTHIA8. The results are obtained in the kinematic region  $|\eta| < 2.4$  and  $0.3 < p_T < 3.0$  GeV.

the proton.

At the same time, the amplitude  $B$  shows a stronger near-side peak in the  $\gamma p$  collisions than pp at the similar  $N_{\text{ch}}$ . The amplitude changes approximately 0.04 to 0.4 from low to high  $N_{\text{ch}}$ . This enhanced near-side peak in  $\gamma p$  collisions originates from the fact that the charge production is governed almost exclusively by a single, short string with strong local charge ordering. In the absence of MPI, minijets, and multiple color strings, the charge-balancing partners remain tightly correlated in  $\Delta\eta$  and  $\Delta\phi$  phase space.

Similarly, the two-dimensional charge-dependent momentum balance correlation  $P_2^{\text{CD}}(\Delta\eta, \Delta\phi)$  is shown in Fig. 4. A distinct feature is seen when comparing pp and  $\gamma p$  collisions. At very low  $N_{\text{ch}}$ , the near-side peak is significantly stronger in  $\gamma p$  interactions than in pp events. This enhancement originates from the single-string topology in  $\gamma p$  collisions, where opposite-charge particles are produced in a more localized manner along the string, resulting in tighter momentum

correlations.

Interestingly, the away-side correlation  $\Delta\phi \approx \pi$  is observed to have similar strength in both systems within the same multiplicity interval. As the event multiplicity increases toward  $N_{\text{ch}} \approx 50$ , the near-side peak, the strengths converge to similar levels between pp and  $\gamma p$  collisions. The results from the  $\gamma p$  collisions with an MB-like tune exhibit qualitatively similar behavior to that observed in the pp collisions. It is found that the  $B$  and  $P_2^{\text{CD}}$  observables show similar multiplicity-dependence, indicating that they depend more strongly on the underlying processes than on the nature of the colliding system.

Overall, a narrower near-side structure in  $P_2^{\text{CD}}$  relative to  $B$  indicates that balancing charges originating from harder partonic processes, such as jet fragmentation, exhibit stronger localized momentum correlations. This difference highlights the complementary sensitivity of the two observables to both the topology and the dynamical properties of particle production.

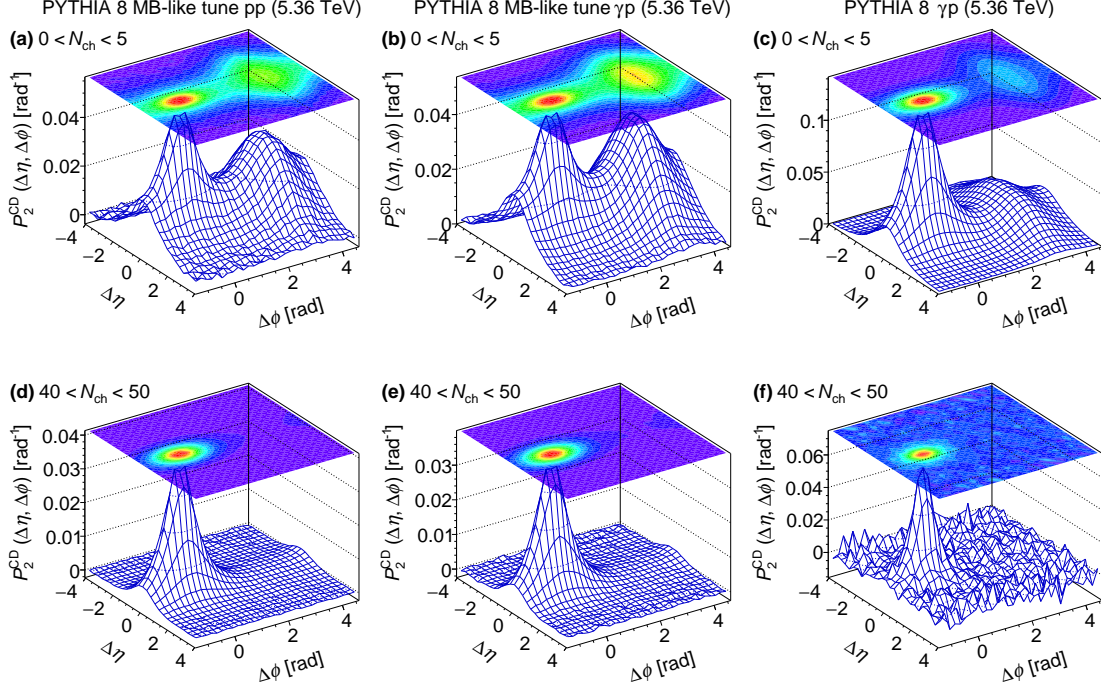


FIG. 4. Two-dimensional momentum balance functions ( $P_2^{\text{CD}}$ ) for  $0 < N_{\text{ch}} < 5$  (upper panel) and  $40 < N_{\text{ch}} < 50$  (lower panel) of charged-hadrons in MB-like tune pp (left), MB-like tune  $\gamma p$  (middle), and  $\gamma p$  (right) collisions at  $\sqrt{s} = 5.36$  TeV from PYTHIA8. The results are obtained in the kinematic region  $|\eta| < 2.4$  and  $0.3 < p_{\text{T}} < 3.0$  GeV.

In addition to the CD correlations, a brief discussion about the CI correlation can be found in Appendix VI.

### B. One-dimensional projections

A clear multiplicity dependence is observed in the 1D distributions of  $B$  as a function of  $\Delta\eta$  and  $\Delta\phi$  for three  $N_{\text{ch}}$  intervals in pp and  $\gamma p$  collisions, as shown in Fig. 5. The near-side peak of the 1D  $B$  distribution becomes narrower with increasing  $N_{\text{ch}}$ . This narrowing is more pronounced in  $\gamma p$  collisions compared to pp collisions. Interestingly, the near side-peak of  $B(\Delta\phi)$  is nearly flat in pp, but a smaller peak-like structure is seen for the  $\gamma p$  at the low  $N_{\text{ch}}$  region. However, at higher  $N_{\text{ch}}$ , a sharper peak is found in  $\gamma p$  than pp collisions.

Figure 6 presents the 1D projections of  $P_2^{\text{CD}}$  along  $\Delta\eta$  and  $\Delta\phi$  direction.  $P_2^{\text{CD}}$  shows a clear multiplicity evolution, and their amplitudes gradually decrease with increasing  $N_{\text{ch}}$ . This behavior reflects due to the combined contribution from

$\langle p_{\text{T}} \rangle$  weight and jet-dominated processes, which is more prominent in low-multiplicity pp events. This trend is opposite to that of the  $B$ . The difference arises because  $P_2^{\text{CD}}$  is sensitive not only to the number of correlated particle pairs but also to their  $p_{\text{T}}$  correlations.

### C. Width comparison

The strength of the correlation between produced hadron pairs is reflected in the width of the balance functions and is quantified by the observables  $\sigma(\Delta\eta)$  and  $\sigma(\Delta\phi)$ , as defined in Eq. 11. Figure 7 shows a clear multiplicity-dependent trend: the widths of  $B$  and  $P_2^{\text{CD}}$  decrease with increasing  $N_{\text{ch}}$  for both pp and  $\gamma p$  collisions.

The extracted widths of these correlations are smaller in  $\gamma p$  collisions than in pp collisions across all multiplicity classes, with the difference becoming more pronounced at higher  $N_{\text{ch}}$ .

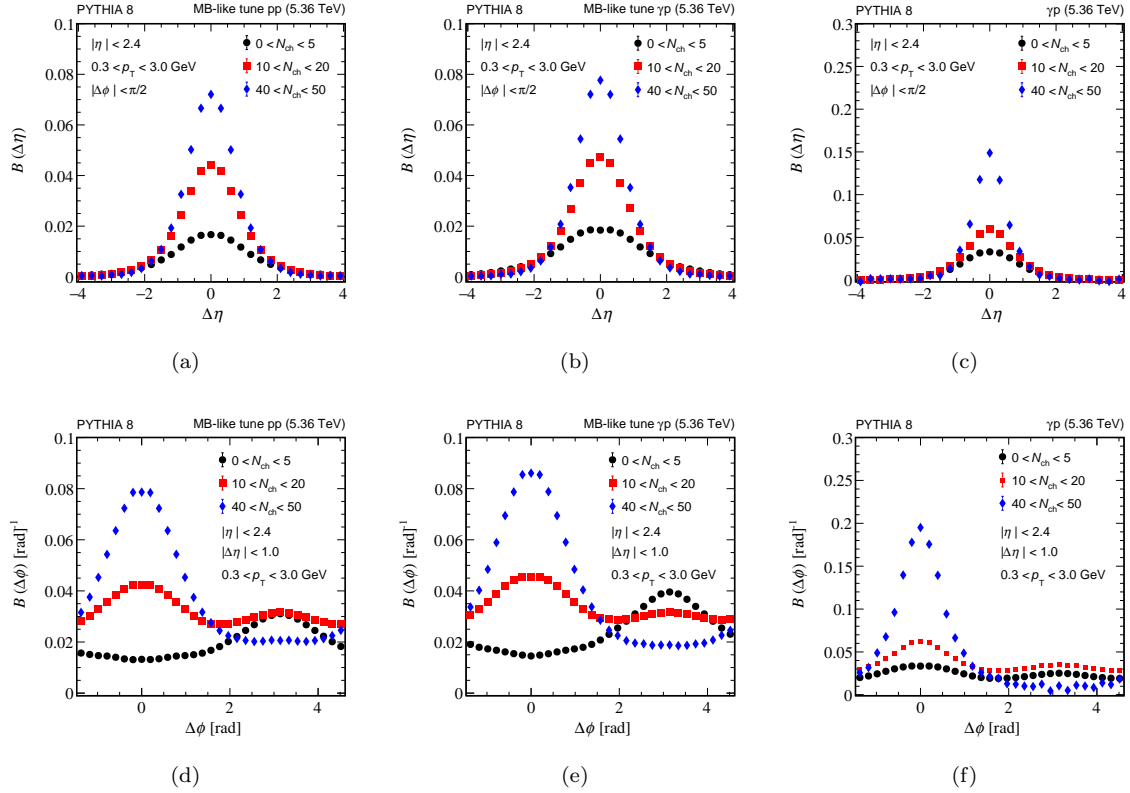


FIG. 5. One-dimensional near-side projection of the number balance functions ( $B$ ) for  $0 < N_{\text{ch}} < 5$  (upper panel) and  $40 < N_{\text{ch}} < 50$  (lower panel) in MB-like tune pp (left), MB-like tune  $\gamma p$  (middle), and  $\gamma p$  (right) collisions at  $\sqrt{s} = 5.36$  TeV from PYTHIA8. The results are obtained in the kinematic region  $|\eta| < 2.4$  and  $0.3 < p_{\text{T}} < 3.0$  GeV for charged-hadrons.

$$\sigma_{P_2^{\text{CD}}(\Delta\eta, \Delta\phi) \text{ or } B(\Delta\eta, \Delta\phi)}^{\gamma p} < \sigma_{P_2^{\text{CD}}(\Delta\eta, \Delta\phi) \text{ or } B(\Delta\eta, \Delta\phi)}^{pp},$$

A comparison of the widths of the  $B$  and  $P_2^{\text{CD}}$ , reveals a clear and systematic dependence on the charged particle multiplicity. The ordering of the widths is preserved across all multiplicity classes,

$$\sigma_{P_2^{\text{CD}}(\Delta\eta, \Delta\phi)} < \sigma_{B(\Delta\eta, \Delta\phi)},$$

suggesting that the underlying mechanisms charge conservation for the balance function and localized jet-like momentum correlations for  $P_2$  remain robust across collision systems. In addition, no significant difference in the extracted widths is observed between  $\gamma p$  and pp collisions when the same PYTHIA8 configuration is used, despite the different colliding systems; however, a small difference appears at low  $N_{\text{ch}}$ . These findings highlight a coherent picture of multiplicity-driven narrowing

in both pp and  $\gamma p$  collisions, while also pointing to open questions regarding the relative strength of MPI, colour reconnection, and hard processes in photon-induced interactions, and how these mechanisms scale with event activity in small systems.

## V. SUMMARY

We present a study of two-particle number ( $B$ ) and transverse-momentum ( $P_2^{\text{CD}}$ ) balance functions of inclusive charged particles as a function of event multiplicity in  $\gamma p$  collisions at LHC energies using PYTHIA8 simulations, and compare the results with pp collisions in the similar multiplicity range. Different PYTHIA8 configurations are considered, including setups with and without inelastic minimum-bias processes, to quantify the role of multiple parton interactions (MPI), string-fragmentation based hadronization and underlying event activities on particle production.

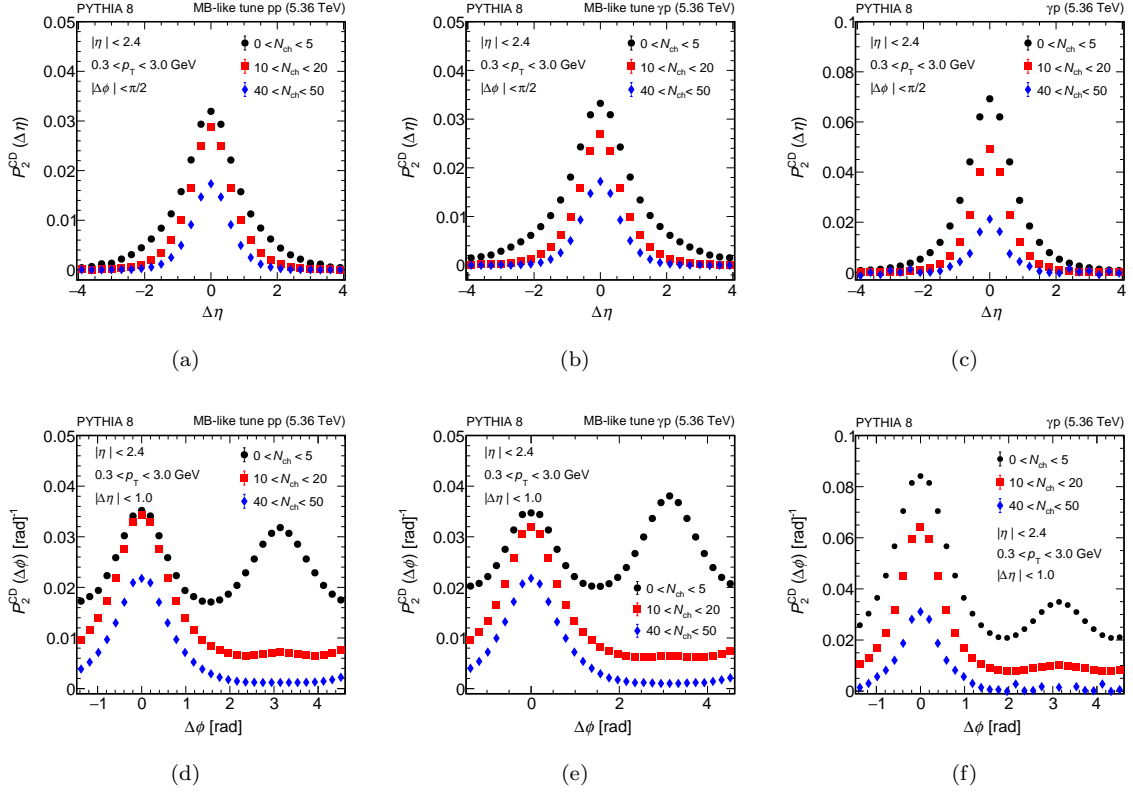


FIG. 6. One-dimensional near-side projection of the momentum balance functions ( $P_2^{\text{CD}}$ ) for  $0 < N_{\text{ch}} < 5$  (upper panel) and  $40 < N_{\text{ch}} < 50$  (lower panel) in MB-like tune pp (left), MB-like tune  $\gamma p$  (middle), and  $\gamma p$  (right) collisions at  $\sqrt{s} = 5.36$  TeV from PYTHIA8. The results are obtained in the kinematic region  $|\eta| < 2.4$  and  $0.3 < p_{\text{T}} < 3.0$  GeV for charged-hadrons.

The widths of both correlation observables decrease with increasing multiplicity in both pp and  $\gamma p$  collisions, demonstrating a clear multiplicity-dependent narrowing. Although photon-induced events populate a lower multiplicity range than hadronic pp interactions, the same trend is present. The comparison at given multiplicity isolates the contribution of hard scattering, the low-multiplicity pp events exhibit a pronounced away-side peak driven by back-to-back dijet production, while such contributions are strongly suppressed in  $\gamma p$  collisions. A dedicated study with identical minimum-bias configurations for pp and  $\gamma p$  collisions shows consistent results, establishing that the observed multiplicity dependence is primarily driven by underlying event activity rather than the initial state.

This behavior in  $\gamma p$  interactions highlights the importance of future experimental measurements

to validate these multiplicity-dependent effects. Future experimental measurements of photon-induced (i.e.,  $\gamma p$ ,  $\gamma \text{Pb}$ ,  $\gamma \text{O}$ ) collisions will therefore provide a clean environment to separate bulk-dominated near-side correlations at low transverse-momentum from jet-driven away-side correlations characteristic of low-multiplicity pp events, delivering a robust baseline for disentangling soft and hard components of particle production across different collision systems.

## ACKNOWLEDGMENTS

S. C. Behera and D. Mallick acknowledge the support under the Istituto Nazionale di Fisica Nucleare (INFN) Postdoctoral Fellowship grant B. C. n. 25865 and B.C. n. 27077.

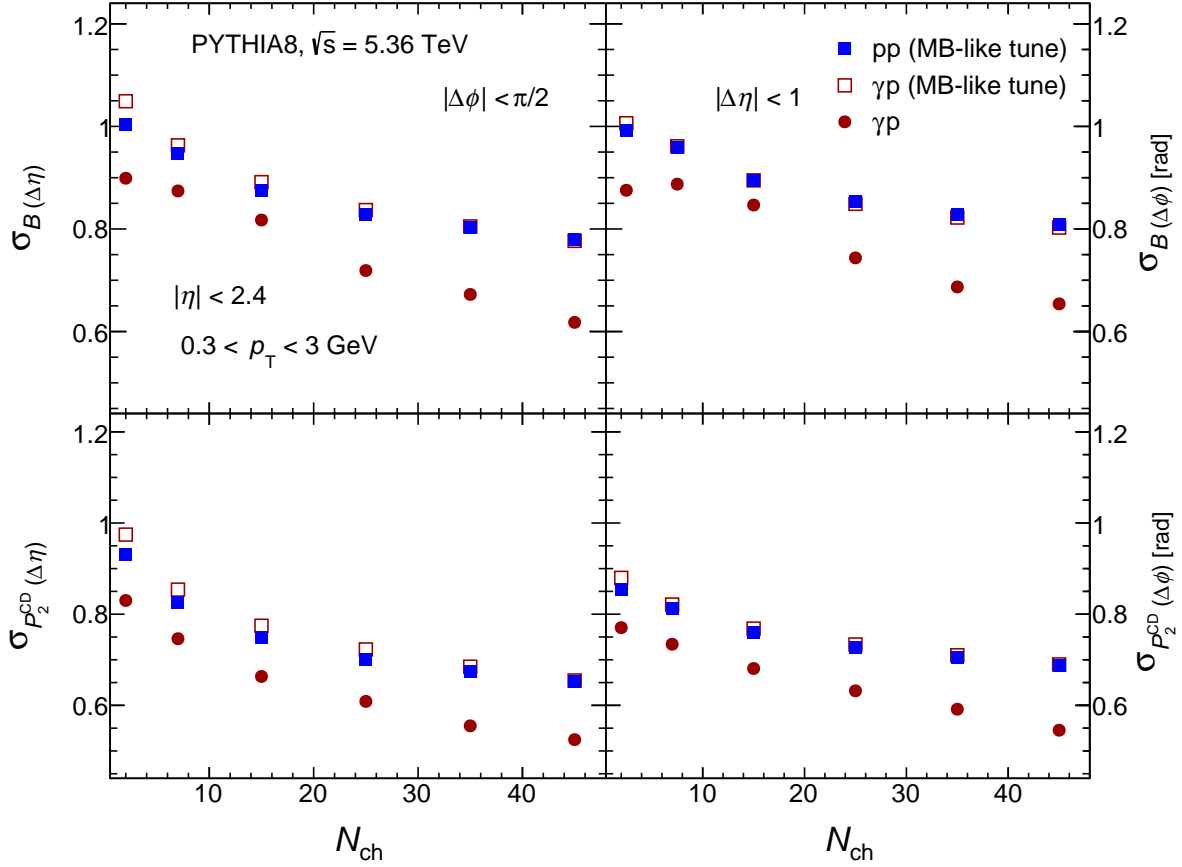


FIG. 7. The RMS width of the number ( $\sigma_B$ ) and momentum ( $\sigma_{P_2^{CD}}$ ) of balance functions in terms of  $\Delta\eta$  (left column) and  $\Delta\phi$  (right column) with  $N_{ch}$ . Both the trigger and associated particles are considered in  $0.3 < p_T < 3.0$  GeV and  $|\eta| < 2.4$  for the charged-hadrons.

- 
- [1] J. W. Harris and B. Muller, “QGP Signatures” Revisited”, *Eur. Phys. J. C* **84** (2024) 247, [arXiv:2308.05743](https://arxiv.org/abs/2308.05743) [hep-ph].
- [2] ALICE Collaboration, S. Acharya *et al.*, “The ALICE experiment: a journey through QCD”, *Eur. Phys. J. C* **84** (2024) 813, [arXiv:2211.04384](https://arxiv.org/abs/2211.04384) [nucl-ex].
- [3] CMS Collaboration, A. Hayrapetyan *et al.*, “Overview of high-density QCD studies with the CMS experiment at the LHC”, *Phys. Rept.* **1115** (2025) 219–367, [arXiv:2405.10785](https://arxiv.org/abs/2405.10785) [nucl-ex].
- [4] BRAHMS Collaboration, I. Arsene *et al.*, “Quark gluon plasma and color glass condensate at RHIC? The Perspective from the BRAHMS experiment”, *Nucl. Phys. A* **757** (2005) 1–27, [arXiv:nucl-ex/0410020](https://arxiv.org/abs/nucl-ex/0410020).
- [5] STAR Collaboration, J. Adams *et al.*, “Experimental and theoretical challenges in the search for the quark gluon plasma: The STAR Collaboration’s critical assessment of the evidence from RHIC collisions”, *Nucl. Phys. A* **757** (2005) 102–183, [arXiv:nucl-ex/0501009](https://arxiv.org/abs/nucl-ex/0501009).
- [6] ALICE Collaboration, “Future high-energy pp programme with ALICE”, <https://cds.cern.ch/record/2724925>. ALICE-PUBLIC-2020-005.
- [7] PHOBOS Collaboration, B. B. Back *et al.*, “The PHOBOS perspective on discoveries at RHIC”, *Nucl. Phys. A* **757** (2005) 28–101, [arXiv:nucl-ex/0410022](https://arxiv.org/abs/nucl-ex/0410022).
- [8] H. Song, S. A. Bass, U. Heinz, T. Hirano, and C. Shen, “200 A GeV Au+Au collisions serve a nearly perfect quark-gluon liquid”, *Phys. Rev.*

- Lett.* **106** (2011) 192301, [arXiv:1011.2783](#) [[nucl-th](#)].
- [9] **ALICE** Collaboration, J. Adam *et al.*, “Multiplicity and transverse momentum evolution of charge-dependent correlations in pp, p–Pb, and Pb–Pb collisions at the LHC”, *Eur. Phys. J. C* **76** (2016) 86, [arXiv:1509.07255](#) [[nucl-ex](#)].
- [10] S. Pratt, “General Charge Balance Functions, A Tool for Studying the Chemical Evolution of the Quark-Gluon Plasma”, *Phys. Rev. C* **85** (2012) 014904, [arXiv:1109.3647](#) [[nucl-th](#)].
- [11] S. A. Bass, P. Danielewicz, and S. Pratt, “Clocking hadronization in relativistic heavy ion collisions with balance functions”, *Phys. Rev. Lett.* **85** (2000) 2689–2692, [arXiv:nucl-th/0005044](#).
- [12] S. Pratt, “Identifying the charge carriers of the quark-gluon plasma”, *Phys. Rev. Lett.* **108** (2012) 212301, [arXiv:1203.4578](#) [[nucl-th](#)].
- [13] S. C. Behera and A. Khuntia, “Jet-associated balance functions of charged and identified hadrons in pp collisions at  $\sqrt{s} = 13.6$  TeV using pythia8”, *Phys. Rev. D* **113** (2026) 032008, [arXiv:2602.03637](#) [[hep-ex](#)].
- [14] **ALICE** Collaboration, S. Acharya *et al.*, “Measurements of differential two-particle number and transverse momentum correlation functions in pp collisions at  $\sqrt{s} = 13$  TeV”, [arXiv:2411.07059](#) [[nucl-ex](#)].
- [15] **ALICE** Collaboration, S. Acharya *et al.*, “Two particle differential transverse momentum and number density correlations in p–Pb and Pb–Pb at the LHC”, *Phys. Rev. C* **100** (2019) 044903, [arXiv:1805.04422](#) [[nucl-ex](#)].
- [16] **ALICE** Collaboration, J. Adam *et al.*, “Multiplicity and transverse momentum evolution of charge-dependent correlations in pp, p–Pb, and Pb–Pb collisions at the LHC”, *Eur. Phys. J. C* **76** (2016) 86, [arXiv:1509.07255](#) [[nucl-ex](#)].
- [17] **STAR** Collaboration, M. M. Aggarwal *et al.*, “Balance functions from au+au, d+au, and p + p collisions at  $\sqrt{s_{NN}} = 200$  gev”, *Phys. Rev. C* **82** (2010) 024905, [arXiv:1005.2307](#) [[nucl-ex](#)].
- [18] **CMS** Collaboration, A. Tumasyan *et al.*, “Multiplicity and transverse momentum dependence of charge-balance functions in pPb and PbPb collisions at LHC energies”, *JHEP* **08** (2024) 148, [arXiv:2307.11185](#) [[nucl-ex](#)].
- [19] **ALICE** Collaboration, B. Abelev *et al.*, “Charge correlations using the balance function in Pb-Pb collisions at  $\sqrt{s_{NN}} = 2.76$  TeV”, *Phys. Lett. B* **723** (2013) 267–279, [arXiv:1301.3756](#) [[nucl-ex](#)].
- [20] C. Pruneau, V. Gonzalez, B. Hanley, A. Marin, and S. Basu, “Accounting for nonvanishing net-charge with unified balance functions”, *Phys. Rev. C* **107** (2023) 014902, [arXiv:2209.10420](#) [[hep-ph](#)].
- [21] C. A. Pruneau, “Role of baryon number conservation in measurements of fluctuations”, *Phys. Rev. C* **100** (2019) 034905, [arXiv:1903.04591](#) [[nucl-th](#)].
- [22] **ALICE** Collaboration, S. Acharya *et al.*, “General balance functions of identified charged hadron pairs of ( $\pi$ ,K,p) in Pb–Pb collisions at  $\sqrt{s_{NN}} = 2.76$  TeV”, *Phys. Lett. B* **833** (2022) 137338, [arXiv:2110.06566](#) [[nucl-ex](#)].
- [23] **CMS** Collaboration, V. Khachatryan *et al.*, “Observation of long-range near-side angular correlations in proton-proton collisions at the LHC”, *JHEP* **09** (2010) 091, [arXiv:1009.4122](#) [[hep-ex](#)].
- [24] **CMS** Collaboration, V. Khachatryan *et al.*, “Measurement of long-range near-side two-particle angular correlations in pp collisions at  $\sqrt{s} = 13$  tev”, *Phys. Rev. Lett.* **116** (2016) 172302, [arXiv:1510.03068](#) [[hep-ex](#)].
- [25] **Belle** Collaboration, Y. C. Chen *et al.*, “Measurement of Two-Particle Correlations of Hadrons in  $e^+e^-$  Collisions at Belle”, *Phys. Rev. Lett.* **128** (2022) 142005, [arXiv:2201.01694](#) [[hep-ex](#)].
- [26] **CMS** Collaboration, S. Chatrchyan *et al.*, “Long-range and short-range dihadron angular correlations in central PbPb collisions at  $\sqrt{s_{NN}} = 2.76$  tev”, *JHEP* **07** (2011) 076, [arXiv:1105.2438](#) [[nucl-ex](#)].
- [27] **CMS** Collaboration, S. Chatrchyan *et al.*, “Observation of long-range, near-side angular correlations in pPb collisions at the LHC”, *Phys. Lett. B* **718** (2013) 795, [arXiv:1210.5482](#) [[nucl-ex](#)].
- [28] **ALICE** Collaboration, S. Acharya *et al.*, “Emergence of long-range angular correlations in low-multiplicity proton-proton collisions”, *Phys. Rev. Lett.* **132** (2024) 172302, [arXiv:2311.14357](#) [[nucl-ex](#)].
- [29] S. C. Behera and A. Khuntia, “Two-particle number and transverse momentum balance function with event-topology in pp collisions at  $\sqrt{s} = 13$  TeV”, [arXiv:2508.20198](#) [[hep-ex](#)].
- [30] S. C. Behera and A. Khuntia, “System size and event shape dependence of particle-identified balance functions in proton-proton collisions at  $\sqrt{s} = 13$  TeV”, [arXiv:2508.21030](#) [[hep-ex](#)].
- [31] B. Sahoo, B. K. Nandi, P. Pujahari, S. Basu, and C. Pruneau, “Simulation studies of  $R_2(\Delta\eta, \Delta\phi)$  and  $P_2(\Delta\eta, \Delta\phi)$  correlation functions in pp collisions with the PYTHIA and HERWIG models”, *Phys. Rev. C* **100** (2019) 024909, [arXiv:1810.09747](#) [[nucl-ex](#)].
- [32] C. Bierlich *et al.*, “A comprehensive guide to the physics and usage of PYTHIA 8.3”, *SciPost Phys. Codeb.* **2022** (2022) 8, [arXiv:2203.11601](#) [[hep-ph](#)].
- [33] **CMS** Collaboration, A. Tumasyan *et al.*, “CMS

- pythia 8 colour reconnection tunes based on underlying-event data”, *Eur. Phys. J. C* **83** (2023) 587, [arXiv:2205.02905 \[hep-ex\]](#).
- [34] CMS Collaboration, A. Tumasyan *et al.*, “Two-particle azimuthal correlations in  $\gamma p$  interactions using pPb collisions at  $\sqrt{s_{NN}}=8.16$  TeV”, *Phys. Lett. B* **844** (2023) 137905, [arXiv:2204.13486 \[nucl-ex\]](#).
- [35] ATLAS Collaboration, G. Aad *et al.*, “Two-particle azimuthal correlations in photonuclear ultraperipheral Pb+Pb collisions at 5.02 TeV with ATLAS”, *Phys. Rev. C* **104** (2021) 014903, [arXiv:2101.10771 \[nucl-ex\]](#).
- [36] C. Bierlich *et al.*, “A comprehensive guide to the physics and usage of PYTHIA 8.3”, *SciPost Phys. Codeb.* **2022** (2022) 8, [arXiv:2203.11601 \[hep-ph\]](#).
- [37] I. Helenius and M. Uthm, “Hadron-ion collisions in Pythia and the vector-meson dominance model for photoproduction”, *Eur. Phys. J. C* **84** (2024) 1155, [arXiv:2406.10403 \[hep-ph\]](#).

## VI. APPENDIX: CHARGE-INDEPENDENT CORRELATIONS

This section presents the charge-independent correlations  $C_2^{CI}$  and  $P_2^{CI}$  for charged hadrons, calculated as the sum of the SS and OS correlations, discussed in Eqs. (7) and (8). Figure 8 shows  $C_2^{CI}$  correlations for charged hadrons in MB pp collisions (left column),  $\gamma p$  collisions with MB-like tune (middle column), and  $\gamma p$  collisions (right column) for two  $N_{ch}$  classes,  $0 < N_{ch} < 5$  (upper panel) and  $40 < N_{ch} < 50$  (lower panel).

For the low- $N_{ch}$ , The near-side CI correlations in MB pp and MB-like  $\gamma p$  exhibit relative suppression with respect to  $\gamma p$  collisions. This behavior can be attributed to the reduced contribution of short-range correlations and multi-particle interactions. A clear near-side enhancement emerges

in all three configurations at higher  $N_{ch}$ . The enhancement with multiplicity is associated with a larger contribution from MPI and semi-hard processes, which strengthen short-range correlations and sharpen the near-side peak, however the away-side structure becomes relatively suppressed.

Similarly, Figure 9 presents CI correlations constructed from the transverse momentum components  $P_2(\Delta\eta, \Delta\phi)$  for two different event configurations. For low-multiplicity events, all these configurations exhibit a localized near-side peak around  $(\Delta\eta, \Delta\phi) \approx (0, 0)$ , indicating short-range correlations dominated by jet fragmentation, resonance decays, and local charge conservation. However, the near-side peak in  $\gamma p$  collisions is visibly stronger and more sharply localized compared to MB pp and MB-like  $\gamma p$ . As the event multiplicity increases, a pronounced enhancement of the near-side peak is observed in both configurations. In contrast, the  $\gamma p$  configuration shows a significantly larger peak magnitude and a reduced away-side structure, indicating that the correlations are dominated by hard scattering processes as the  $\langle p_T \rangle$  increases.

The CI and CD correlations of  $C_2$  and  $P_2$  are studied for charged hadrons in pp and  $\gamma p$  collisions. A similar behavior is observed for both CI and CD results, however, the amplitude of the CI correlations is larger than that of the CD correlations because the CI component includes contributions from both SS and OS pairs. This suggests that the final CI correlation strength arises from various physics processes, such as jet fragmentation, resonance decays, the Hanbury Brown–Twiss (HBT) effect, local charge conservation (LCC), and other global event properties. In addition, the near-side peak of  $P_2^{CI}$  is found to be narrower than  $C_2^{CI}$ . This behavior is consistent with the angular ordering of the  $p_T$ , where produced particles exhibit stronger localized momentum correlations. Similar behavior is also expected from hadronic resonance decays as discussed in Ref. [14, 15, 29].

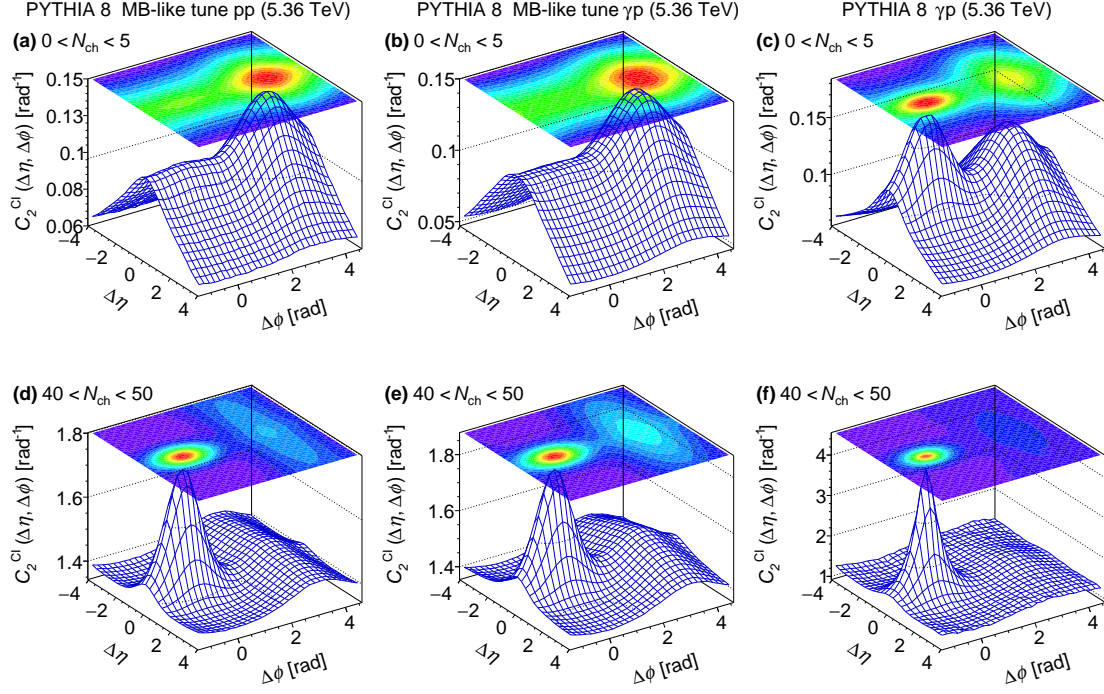


FIG. 8. Two-dimensional charge-independent number correlations ( $C_2^{\text{CI}}$ ) for  $0 < N_{\text{ch}} < 5$  (upper panel) and  $40 < N_{\text{ch}} < 50$  (lower panel) in MB-like tune pp (left), MB-like tune  $\gamma p$  (middle), and  $\gamma p$  (right) collisions at  $\sqrt{s} = 5.36$  TeV from PYTHIA8. The results are obtained in the kinematic region  $|\eta| < 2.4$  and  $0.3 < p_{\text{T}} < 3.0$  GeV charged-hadrons.

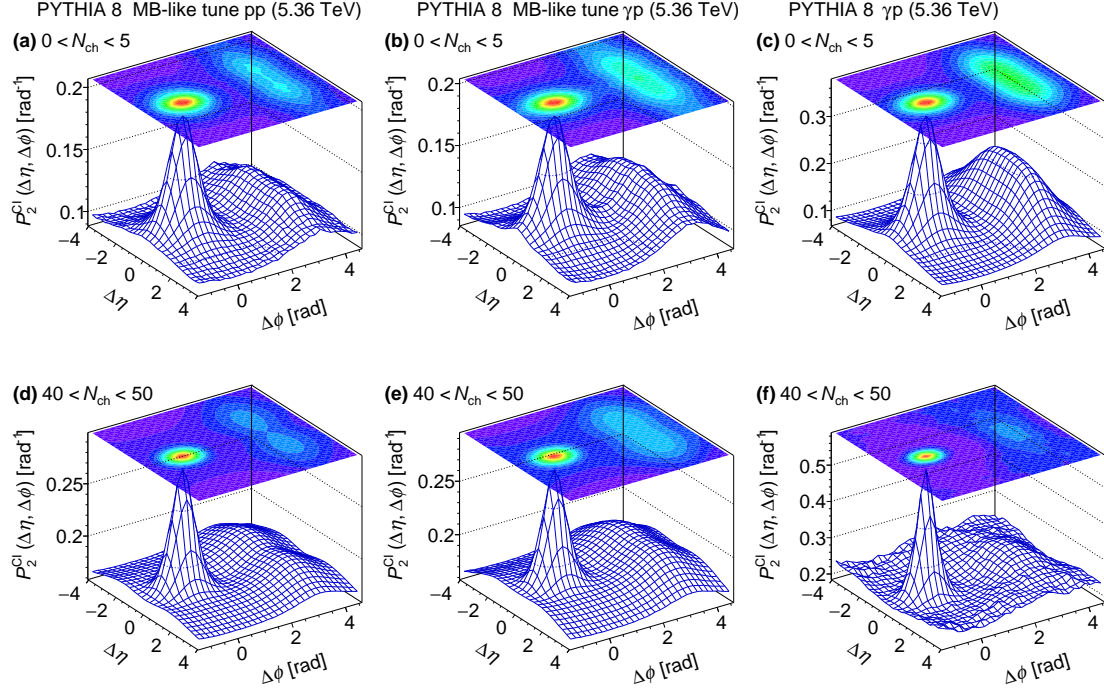


FIG. 9. Two-dimensional charge-independent momentum correlations ( $P_2^{\text{CI}}$ ) for  $0 < N_{\text{ch}} < 5$  and  $40 < N_{\text{ch}} < 50$  in MB-like tune pp (left), MB-like tune  $\gamma$ p (middle), and  $\gamma$ p (right) collisions at  $\sqrt{s} = 5.36$  TeV from PYTHIA8. The results are obtained in the kinematic region  $|\eta| < 2.4$  and  $0.3 < p_{\text{T}} < 3.0$  GeV for charged-hadrons.